

Field Theoretic Study of Bilayer Membrane
Fusion III: Membranes with Leaves of
Different Composition

J.-Y. Lee and M. Schick
Department of Physics
University of Washington, Box 351560, Seattle, WA 98195-1560

Abstract

We extend previous work on homogeneous bilayers to calculate the barriers to fusion of planar bilayers which contain two different amphiphiles, a lamellae-former and a hexagonal former, with different compositions of the two in each leaf. Self-consistent field theory is employed, and both standard and alternative pathways are explored. We first calculate these barriers as the amount of hexagonal former is increased equally in both leaves to levels appropriate to the plasma membrane of human red blood cells. We follow these barriers as the composition of hexagonal-formers is then increased in the cis layer and decreased in the trans layer, again to an extent comparable to the biological system. We find that, while the fusion pathway exhibits two barriers in both the standard and alternative pathways, in both cases the magnitudes of these barriers are comparable to one another, and small, on the order of $13 k_B T$. As a consequence, one expects that once the bilayers are brought sufficiently close to one another to initiate the process, fusion should occur rapidly.

1 Introduction

In spite of the importance of membrane fusion to biological processes such as endocytosis, intra-cell trafficking, and viral infection, and in spite of the increased attention devoted to it, the process is still not well understood. In particular, it is unclear what the sequence of events along the path to fusion is, which of those events presents the greatest barrier to fusion, and what the magnitude of that barrier is.

The initial stages of the sequence are relatively clear (1, 2). The membranes to be fused must be brought sufficiently close to one another, within a few nanometers. In order to do so, water must be removed, which takes energy. Presumably this is provided by fusion proteins in biological systems, but can, in laboratory ones in which such proteins are absent, be provided simply by ordinary depletion forces (3). As a result of the decrease of water, the free energy per unit area of the system increases; in other words, the system is now under tension. The free energy can be reduced if the system sheds area. Fusion, which accomplishes this, is one possible response of the system to that tension. The next stage in the process is that, locally, some lipid tails in the membrane leaves which are closest to one another, the cis leaves, flip over and embed themselves in the hydrophobic environment of the cis leaf of the other bilayer, thereby forming a “stalk” (4), as depicted in Fig. 1(a). This process is consistent with experimental evidence ((1) and references therein), and has been seen directly in simulations of coarse-grained, microscopic, models of membranes (5–9).

The next stage is unclear, and several possibilities have been proposed. The original suggestion (4) was that the stalk expands radially from an axis perpendicular to the bilayers, as in Fig. 1(b). The cis layers retract leaving a hemifusion diaphragm which consists only of the leaves of the two membranes which were initially furthest from one another, the trans leaves. Note that membrane area has been reduced as the hemifusion diaphragm now consists only of two, trans, leaves in place of the original four, two cis and two trans. The appearance of a hole in this hemifusion diaphragm completes the formation of the fusion pore, Fig. 1(c). On the basis of phenomenological modeling similar to that employed earlier (4), a second scenario was suggested: that the pore forms without significant radial expansion of the stalk (10, 11). A third possibility was revealed by simulations of coarse-grained, microscopic models (5, 6, 12). In this, which we denote the first stalk-hole mechanism, the stalk does not expand radially, but elongates asymmetrically. Its presence makes

more favorable the formation nearby of a hole in either bilayer by reducing the line tension of the hole (13). The stalk then surrounds the hole which also produces a hemifusion diaphragm, as in the standard stalk mechanism, but one which consists here of a cis and trans layer of one of the original bilayers. The appearance of a second hole, this in the hemifusion diaphragm, then completes the fusion pore. A hemifusion diaphragm is also consistent with experimental evidence ((14) and references therein.) In a variant of this mechanism, denoted the second stalk-hole mechanism, the second hole appears before the first is surrounded. The mobile stalk then surrounds them both forming the fusion pore. After formation of the fusion pore, the pore expands to further eliminate area and thus reduce the system's free energy. Simulations of coarse-grained, microscopic, models have observed the original mechanism (8, 9, 12), and also the stalk-hole mechanism (5–9, 12). If the path to fusion is not well established, neither is the limiting free energy barrier of the process. It had been thought, on the basis of phenomenological calculations, that the free energy to form the initial stalk was so large, that its formation could well be the barrier to fusion. Improvements in the way the stalk was modeled (15), and in the phenomenological free energy describing the elastic properties of the membrane (16) which forms the stalk, resulted in a marked reduction in the estimate of the free energy of formation of the stalk. For a bilayer with symmetric leaves characterized by a spontaneous curvature appropriate to dioleoylphosphatidylcholine (DOPC), this quantity is estimated by Kozlovsky and Kozlov (16) to be $43k_B T$, and by Kuzmin et al. (11) to be about $25k_B T$. In contrast to phenomenological theories, self-consistent field theory has been applied to a coarse-grained microscopic model of a symmetric membrane (17), resulting in an even lower estimate of $13k_B T$. Irrespective of the particular number, it would not appear that the formation of the stalk presents the largest barrier to fusion.

If stalk formation is not the rate limiting process in fusion, what is? In the standard picture in which the stalk expands radially into a hemifusion diaphragm, it is the formation of this structure which takes a great deal of energy. For a symmetric bilayer of DOPC, a diaphragm of modest radius of 2.5nm costs on the order of $80k_B T$, if one uses the estimate of Kozlovsky and Kozlov (16) for the diaphragm line tension. How large the diaphragm must become before a pore forms is not clear from this calculation. Kuzmin et al. (11) consider a modified stalk and a different radial symmetric intermediate, a pre-pore. They find its energy, about $60 k_B T$, to be less than that of a hemifusion diaphragm, and the largest along the fusion pathway. Self-

consistent field calculations examined both the classical pathway (17) and the first stalk-hole mechanism (13), and located the barriers to fusion for symmetric bilayers. In the former, the largest barrier occurred when the hemifusion diaphragm expanded to a radius which was of the same order of the hydrophobic thickness of a bilayer. Pore formation followed. The value of the barrier ranged from about 25 to 65 $k_B T$, depending upon the tension and the architecture of the amphiphiles. The barrier decreases with increasing tension and as the architecture tends toward dioleoylphosphatidylethanolamine, DOPE, and away from DOPC. Calculated barriers in the stalk-hole mechanism tended to be somewhat smaller than in the standard mechanism, but only by a few $k_B T$. Thus the two mechanisms seem to be comparable in terms of their energetics, at least for the symmetric membranes examined.

Biological membranes are not symmetric, however. In human red blood cell membranes, for example, most of the cholinephospholipids, sphingomyelin (SM) and phosphatidylcholine (PC), are found in the outer, ectoplasmic, leaf, and most of the aminophospholipids, phosphatidylethanolamine (PE) and phosphatidylserine (PS), are found in the inner, cytoplasmic, leaf (18, 19). In particular the mole percent of PC in the outer/inner leaf is 22/8, of SM is 20/5, of PS is 0/10, and of PE is 8/27 (18). To maintain this imbalance costs energy (20), therefore it is reasonable to assume that it plays some physiological function. One suggestion is that this imbalance promotes fusion in intracellular events (21–23). The reasoning is as follows. Of the four major lipid groups cited above, three of them, SM, PC, and PS (24) form bilayers under physiological conditions. They make up 65% of the total bilayer, but 84% of the outer, trans, leaf. PE, however, does not form lamellae, but rather an inverted hexagonal phase (25). It has often been noted (26) that regions of this non-bilayer phase resemble the non-bilayer configurations posited to occur in fusion. Furthermore, PE resides predominantly in the inner, cytoplasmic, leaf of the plasma membrane. While it makes up only 35% of the total bilayer composition of human red blood cell membranes, it comprises 54% of the inner leaf. It is presumed to also reside predominantly in the outer leaf of a bilayer vesicle within the cell, as the outer leaf of such a vesicle would make contact with the inner leaf of the plasma membrane during fusion of the vesicle and plasma membrane, and thereby have the opportunity to exchange lipid content. But it is precisely the inner leaf of the plasma membrane and the outer leaf of a vesicle which would be closest to one another during fusion (i.e. would be the cis leaves), and would undergo the largest deviation from a planar configuration. Hence the enhanced concentration of PE in these

leaves would presumably promote fusion.

There is much experimental evidence to support the view that the presence of hexagonal-forming lipids in the cis leaves enhances fusion. In particular, model membranes (i.e. which have equal composition in both leaves) fuse readily when composed of a mixture of PE and PS approximating that of the inner leaf of the erythrocyte membrane (27), while those consisting of PC and SM do not. Asymmetric membranes were investigated by Eastman et al. (21) who utilized dioleoylphosphatidic acid (DOPA), a lipid with a head group smaller even than PE, which they could move from cis to trans layers by applications of a pH gradient. When DOPA was present in the cis layers in modest amounts, 5 mol percent, fusion of large unilamellar vesicles occurred readily on the addition of Ca^{2+} . However when DOPA was sequestered in the trans monolayer, little or no fusion was observed. Conversely, if one adds to the cis layer lauroyl lysophosphatidylcholine, which has a large head group when compared to its single tail, fusion is inhibited dramatically (23).

As important as this asymmetry appears to be to the process of fusion, it is little addressed in theoretical calculations. In phenomenological ones, it has been accounted for by allowing the inner and outer leaves to be characterized by different spontaneous curvatures. In this way Kozlovsky and Kozlov (16) predict that the free energy of stalk formation depends essentially only on the spontaneous curvature of the cis leaves, and decreases rapidly as this curvature is made more negative, (i.e. as one proceeds from the lamellae-formers towards the hexagonal -formers). A similar calculation and result follows for the free energy of formation of the hemifusion diaphragm (28). There are no direct results for the effect of the asymmetry on the largest barrier to fusion. However, by treating the entire cis layer as having the same spontaneous curvature, the calculation cannot capture the effect that hexagonal forming lipids can respond *locally* to an environment in which the leaves are locally deformed i.e. where their distribution, in general, is not uniform (29). Simulations of fusion have not yet considered the effects of asymmetry, presumably because the asymmetric distribution represents a constrained equilibrium, a situation more difficult to handle than an unconstrained one.

In this paper, we extend the application of self-consistent field theory to microscopic models of membranes (13, 17) and consider two important effect noted above; that the bilayer leaves consist of at least two classes of lipids, lamellae-formers and hexagonal-formers, and that these lipids are distributed asymmetrically with respect to the cis and trans layers. We shall deal with these effects in two stages. First we consider the effect on

the barriers to fusion due to the presence of two kinds of amphiphiles in leaves of identical composition, as in artificial membranes. We do this for the standard mechanism, and for both the first and second stalk-hole fusion mechanisms. We find that the barriers are reduced appreciably because the hexagonal-forming amphiphiles can go to the regions where they relieve the most strain (29). The barriers in the two variants of the stalk-hole mechanism are not very different from one another. We then consider the same overall composition, but redistribute the two amphiphiles asymmetrically, with the hexagonal-formers being more concentrated in the cis leaves. The barriers in the standard fusion mechanism and in the second stalk-hole mechanism are calculated. The overall effect of having two such different amphiphiles distributed unequally between the two leaves is dramatic. The major barriers to fusion in the two scenarios are reduced to such an extent that they are now comparable to the rather small initial barrier to stalk formation. This barrier is not affected appreciably by the addition of the hexagonal-formers nor by their asymmetric distribution, and remains on the order of $13 k_B T$. As a result, the fusion pathway consists of two small barriers. Once bilayers are brought sufficiently close to initiate the process, fusion should therefore proceed rapidly.

2 The model

The model is similar to that employed earlier (13, 17), so we will only discuss here the necessary extensions. We consider a system of two different amphiphiles, AB block copolymers, denoted 1 and 2, and solvent of A homopolymer. The volumes occupied by a solvent chain of N segments, and of a chain of amphiphile 1, also taken to be of N segments, are Nv , where v is the volume of each segment. The volume occupied by a chain of amphiphile 2 of $\tilde{\alpha}N$ segments is $\tilde{\alpha}Nv$. The fraction of hydrophilic, A, monomers in amphiphile 1 is f_1 and that in amphiphile 2 is f_2 . In our subsequent calculations we shall take $f_1 = 0.4$, close to the value of 0.43 which would characterize DOPC, and $f_2 = 0.294$, approximately the value characterizing DOPE (17). In order that the hydrophobic length of the two different amphiphiles be the same, we require $(1 - f_1)Nv = (1 - f_2)\tilde{\alpha}Nv$ so that $\tilde{\alpha} = 0.85$. Thus we have two amphiphiles with the same hydrophobic length, but different hydrophilic lengths. Amphiphile 2 is a hexagonal-former with a smaller hydrophilic head group than amphiphile 1, which is a lamellae-former. We denote the local

volume fraction of hydrophilic elements of amphiphile 1 to be $\phi_{A,1}(\mathbf{r})$, of amphiphile 2 to be $\phi_{A,2}(\mathbf{r})$, and of the solvent to be $\phi_{A,s}(\mathbf{r})$. The total local volume fraction of hydrophilic elements is denoted

$$\phi_A(\mathbf{r}) = \phi_{A,1}(\mathbf{r}) + \phi_{A,2}(\mathbf{r}) + \phi_{A,s}(\mathbf{r}). \quad (1)$$

Similarly the total local volume fraction of hydrophobic elements is

$$\phi_B(\mathbf{r}) = \phi_{B,1}(\mathbf{r}) + \phi_{B,2}(\mathbf{r}). \quad (2)$$

The amounts of each of the components are controlled by activities, z_1 , z_2 , and z_s . The system is taken to be incompressible and of volume V . Because of the incompressibility constraint, only two of the activities are independent. Within the self-consistent field approximation, the excess free energy, $\delta\Omega^{sym}(T, A, z_1, z_2, z_s)$, of the bilayer system of area A , is given by

$$\begin{aligned} \frac{Nv}{k_B T} \delta\Omega^{sym} &= -z_1 Q_1 - z_2 Q_2 - z_s Q_s \\ &+ \int d\mathbf{r} [\chi N \phi_A(\mathbf{r}) \phi_B(\mathbf{r}) - w_A(\mathbf{r}) \phi_A(\mathbf{r}) - w_B(\mathbf{r}) \phi_B(\mathbf{r}) \\ &- \xi(\mathbf{r})(1 - \phi_A(\mathbf{r}) - \phi_B(\mathbf{r}))], \end{aligned} \quad (3)$$

where $Q_1(T, [w_A, w_B])$, $Q_2(T, [w_A, w_B])$, and $Q_s(T, [w_A])$ are the configurational parts of the single chain partition functions of amphiphiles 1 and 2 and of solvent. They have the dimensions of volume, and are functions of the temperature, T , which is inversely related to the Flory interaction χ , and functionals of the fields w_A and w_B . These fields, and the Lagrange multiplier $\xi(\mathbf{r})$, which enforces the local incompressibility condition, are determined by the self-consistent equations

$$w_A(\mathbf{r}) = \chi N \phi_B(\mathbf{r}) + \xi(\mathbf{r}), \quad (4)$$

$$w_B(\mathbf{r}) = \chi N \phi_A(\mathbf{r}) + \xi(\mathbf{r}), \quad (5)$$

$$1 = \phi_A(\mathbf{r}) + \phi_B(\mathbf{r}), \quad (6)$$

$$\phi_A(\mathbf{r}) = -z_1 \frac{\delta Q_1[w_A, w_B]}{\delta w_A(\mathbf{r})} - z_2 \frac{\delta Q_2[w_A, w_B]}{\delta w_A(\mathbf{r})} - z_s \frac{\delta Q_s[w_A]}{\delta w_A(\mathbf{r})}, \quad (7)$$

$$\phi_B(\mathbf{r}) = -z_1 \frac{\delta Q_1[w_A, w_B]}{\delta w_B(\mathbf{r})} - z_2 \frac{\delta Q_2[w_A, w_B]}{\delta w_B(\mathbf{r})}. \quad (8)$$

The partition functions are obtained from the solution of a modified diffusion equation, as detailed as in the first paper in this series (17), and the barriers

to fusion are calculated for the standard and for the stalk/hole mechanisms as in the previous two papers (13, 17). The free energy in the self consistent field approximation, $\delta\Omega_{scf}^{sym}$, is obtained by inserting into the free energy of Eq. 3 the functions which satisfy the self-consistent equations 4-8 with the result

$$\begin{aligned} \frac{Nv}{k_B T} \delta\Omega_{scf}^{sym}(T, A, z_1, z_2, z_s) &= -z_1 Q_1(T, [w_A, w_B]) - z_2 Q_2(T, [w_A, w_B]) \\ &- z_s Q_s(T, [w_A]) - \int d\mathbf{r} \chi N \phi_A(\mathbf{r}) \phi_B(\mathbf{r}), \end{aligned} \quad (9)$$

where we have set $\int \xi(\mathbf{r}) d\mathbf{r} = 0$.

Calculation of the barrier to fusion in the standard mechanism is relatively straightforward because all intermediates, the stalk, hemifusion diaphragm, and pore, are characterized by axial symmetry about the z axis, and reflection symmetry in the xy plane. The former symmetry is absent in the intermediates of the stalk-hole mechanisms. In order to make tractable the calculation of the barrier along this path, the actual intermediates were approximated by intermediates constructed from segments of configurations which possessed both symmetries and whose free energy, therefore, were easily obtained (13).

Just before formation of the stalk-hole complex, the elongated stalk was treated as if it were in the shape of a circular arc with a fractional angle, $0 \leq \alpha \leq 1$, and radius R , as shown schematically in Fig. 2(a). Its free energy is

$$F_1(R, \alpha) = \alpha F_{IMI}(R) + F_s, \quad (10)$$

where F_{IMI} is the energy of the structure shown at the extreme right of Fig. 2(a) which corresponds to $\alpha = 1$, and F_s is the free energy of a stalk. This is because it is the sum of the energies of the two end caps of a structure for which $\alpha \neq 1$, and these two end caps together make a stalk.

Just after formation of the stalk-hole complex in the first stalk-hole mechanism, there is a hole in one of the two bilayers (30–34). which is partially surrounded by the elongated stalk. This intermediate is approximated by the configuration shown in Fig. 2(b) whose free energy is

$$F_2(R, \alpha) = \alpha F_{HI}(R) + (1 - \alpha) F_H(R - \delta) + F_d. \quad (11)$$

Here F_{HI} is the free energy of the structure with $\alpha = 1$ in which the stalk would have completely surrounded the hole forming a hemifusion intermediate, $F_H(R - \delta)$ is the free energy of a hole of radius $R - \delta$ in a bilayer, and

F_d is the free energy of the defects at the end of the arc. Equality of the free energies of Eqs. 10 and 11 defines a ridge line in the space of parameters α and R , and the minimum of this ridge defines a saddle point along this fusion path.

In the second stalk-hole mechanism, just after formation of the stalk-hole complex, there are two holes, one in each bilayer, partially surrounded by the elongated stalk. Again the picture is as in Fig. 2(b), but now the circular object in the center of the figure represents the *two* holes, rather than the one as previously. Thus the figure at the extreme right now represents a fusion pore. The free energy of this configuration is

$$F_3(R, \alpha) = \alpha F_{pore}(R) + (1 - \alpha) F_{2H}(R - \delta) + F'_d. \quad (12)$$

Here $F_{pore}(R)$ is the free energy of a pore of radius R , $F_{2H}(R - \delta) = 2F_H(R - \delta)$ is the free energy of two holes, each of radius $R - \delta$, one above the other, and F'_d the energy of the two defects at the end of the arc. Again equality of Eqs. 10 and 12 defines a ridge line in the space of parameters α and R . The minimum along this ridge defines the fusion barrier along this second stalk-hole pathway.

3 Results for symmetric bilayers

We first show in Fig. 3 how the addition of the hexagonal-forming amphiphiles affect the barrier to fusion in the standard mechanism. We plot there in solid lines the free energy of the stalk which expands into a hemifusion diaphragm as a function of the structure's radius divided by the radius of gyration, R_g , of the larger amphiphile. (The hydrophobic thickness of a single bilayer composed of amphiphiles with $f = 0.4$ is $2.7 R_g$.) When the radius is smaller than about $0.5 R_g$, we find no stable stalk solution of the self-consistent equations. We have taken the volume Nv which appears in the free energy, Eq. 9, to be $Nv = 1.54R_g^3$, as in our previous work (13, 17). The four solid curves in Fig. 3 correspond to volume fractions of the hexagonal-former of 0, 0.04, 0.11, and 0.17 from top to bottom. The dotted curves show the free energies of fusion pores for the same volume fractions. We take the barrier to fusion to be that value at which the free energies of a hemifusion diaphragm and fusion pore of the same radius are equal. The bilayer is under a tension of $\gamma/\gamma_0 = 0.2$, where γ_0 is the interfacial free energy per unit area between coexisting solutions of hydrophobic and hydrophilic homopolymers

at the same temperature. At larger values of the radius of the hemifusion diaphragm than shown in the figure, the free energy of the diaphragm decreases due to the tension. One sees from Fig. 3 that the barrier to fusion does indeed decrease with the addition of hexagonal-formers. As can be seen in the figure, this reduction comes about both because of the reduction in energy of the fusion pore and of the hemifusion diaphragm. The reduction in the pore energy is due to the effect of the hexagonal-formers which can go to the sharp bend of the cis leaf existing in the pore. Similarly the reduction in the energy of the hemifusion diaphragm is due to the hexagonal-formers concentrating at the rim of the diaphragm. This is shown in Fig. 4. In (a) the volume fractions of the heads, dashed line, and tails, solid line, of the hexagonal-forming amphiphile far from the hemifusion diaphragm are shown as a function of z/R_g . In (b) we show the volume fractions of the hexagonal-forming amphiphile in a cut through the hemifusion diaphragm itself in the plane of reflection symmetry, the $z = 0$ plane, as a function of the radial coordinate, ρ/R_g . (Recall that such a hemifusion diaphragm is shown in Fig. 1(b).) One sees that the diaphragm has an approximate radius of $5R_g$. A comparison of plots (a) and (b) shows that the *local* volume fraction of tails of the hexagonal-former at the diaphragm rim increases by about 20 %, and that the *local* density of heads of this amphiphile increases there by almost 50%.

The barrier to fusion in the standard mechanism is shown in the upper curve of Fig. 5 as a function of concentration of the hexagonal-forming amphiphile. One sees that the dependence is non-linear. The effect of the hexagonal-forming amphiphile in reducing the barrier to fusion is greatest when this amphiphile is first added, as it can go to the region where it relieves the most strain. As more and more is added, its ability to reduce the barrier to fusion is lessened.

The barrier to fusion in the first stalk-hole mechanism is shown in the lower curve. We have assumed a reasonable energy of $4 k_B T$ for the defects that appear at the end of the elongated stalk which partially surrounds a hole in one of the bilayers. That the barrier to fusion is somewhat lower in the first stalk-hole mechanism than in the standard one, and is much less sensitive to the architecture than is the standard mechanism for a system composed primarily of amphiphile characterized by $f = 0.4$ could have been anticipated by the results presented in Fig. 10 of reference (13). As seen there, for $f = 0.35$, and $\gamma/\gamma_0 = 0.2$, the barrier to fusion is somewhat lower in the first stalk-hole mechanism than in the standard mechanism, and the

barrier in the latter varies more rapidly with architecture, f , than in the stalk-hole mechanism.

In the upper panel of Fig. 6, we compare the fusion barriers in the first and second stalk mechanisms. The former is shown in filled circles and the latter is shown in filled triangles. Defect energies are taken to be $4 k_B T$. One sees that there is not a great deal of difference in the energy barriers in the two mechanisms. One also notes that the second stalk-hole mechanism has a lower energy than that of the first when the fraction of hexagonal-forming amphiphiles is low. The situation is reversed as the fraction increases. This is to be expected as the second stalk-hole intermediate consists of portions of a fusion pore and of two holes. Both of these structures are disfavored by the hexagonal-forming amphiphiles. On the other hand, the first stalk-hole intermediate consists of portions of a hemifusion diaphragm, and only one hole. The hemifusion diaphragm is favored by the hexagonal-forming amphiphiles.

The lower panel of Fig. 6 illustrates that the barrier to fusion in the stalk-hole mechanism is not very sensitive to the choice of defect energy. The barrier heights are shown there for the first stalk-hole mechanism for the case in which the defect energy is $4k_B T$ (open circles) and in which the defect energy vanishes (closed circles).

4 Results for asymmetric bilayers

We now consider the situation in which the compositions of the two different leaves of the bilayer differ. In particular, we will fix the composition of the hexagonal-forming lipid in the cis leaf. The overall composition of lamellae- and hexagonal-forming lipids in the bilayer is still controlled by the activities z_1 , z_2 and z_s and the incompressibility condition. Therefore we want to calculate the excess free energy $\delta\Omega^{asym}(T, A, z_1, z_2, z_s, n_2^{cis})$, where n_2^{cis} is the number of hexagonal-forming lipids in the cis leaf of the bilayer;

$$\begin{aligned} n_2^{cis} &= \frac{1}{\alpha N v} \int d\mathbf{r} \phi_2(\mathbf{r}), \\ &= \frac{1}{\alpha N v f_2} \int d\mathbf{r} \phi_{A,2}(\mathbf{r}). \end{aligned} \quad (13)$$

The integral is over the volume of the cis leaf of the bilayer. In the second line, we determine the number of hexagonal-forming lipids in the cis layer by

counting the number of their head groups, which will be more convenient. Rather than calculate the free energy in an ensemble in which the number of hexagonal-forming lipid heads is fixed, it is far easier, as usual, to calculate the free energy in an ensemble in which a local field, $h(\mathbf{r})$, controls the average local average value of $\phi_{A,2}(\mathbf{r})$, and therefore of n_2^{cis} . This adds to the system's internal energy a term of the form

$$-\frac{k_B T}{Nv} \int d\mathbf{r} h(\mathbf{r}) \phi_{A,2}(\mathbf{r}) \quad (14)$$

The field $h(\mathbf{r})$ is taken to be non-zero only in the cis leaf, and will be discussed further below. By a simple extension of the procedure for the symmetric bilayer we obtain for the excess free energy in this ensemble, $\delta\tilde{\Omega}^{asym}(T, A, z_1, z_2, z_s, [h])$,

$$\begin{aligned} \frac{Nv}{k_B T} \delta\tilde{\Omega}^{asym} &= -z_1 Q_1(T, [w_A, w_B]) - z_2 Q_2(T, [w_A - h, w_B]) - z_s Q_s(T, [w_A]) \\ &+ \int d\mathbf{r} [\chi N \phi_A(\mathbf{r}) \phi_B(\mathbf{r}) - w_A(\mathbf{r}) \phi_A(\mathbf{r}) - w_B(\mathbf{r}) \phi_B(\mathbf{r}) \\ &- \xi(\mathbf{r})(1 - \phi_A(\mathbf{r}) - \phi_B(\mathbf{r}))]. \end{aligned} \quad (15)$$

The self-consistent equations, 4 to 8, are unaffected. Again the free energy in the self-consistent field approximation is obtained by substituting the functions which satisfy the self-consistent equations into the free energy of Eq. 15 with the result

$$\begin{aligned} \frac{Nv}{k_B T} \delta\tilde{\Omega}_{scf}^{asym} &= -z_1 Q_1(T, [w_A, w_B]) - z_2 Q_2(T, [w_A - h, w_B]) - z_s Q_s(T, [w_A]) \\ &- \int d\mathbf{r} \chi N \phi_A(\mathbf{r}) \phi_B(\mathbf{r}), \end{aligned} \quad (16)$$

The desired free energy, $\delta\Omega_{scf}^{asym}(T, A, z_1, z_2, z_s, n_2^{cis})$, is now obtained by a Legendre transform

$$\begin{aligned} \frac{Nv}{k_B T} \delta\Omega_{scf}^{asym}(T, A, z_1, z_2, z_s, n_2^{cis}) &= \frac{Nv}{k_B T} \delta\tilde{\Omega}_{scf}^{asym}(T, A, z_1, z_2, z_s, [h]) \\ &+ \int d\mathbf{r} h(\mathbf{r}) \phi_{A,2}(\mathbf{r}) \end{aligned} \quad (17)$$

so that

$$\begin{aligned} \frac{Nv}{k_B T} \delta\Omega_{scf}^{asym} &= -z_1 Q_1(T, [w_A, w_B]) - z_2 Q_2(T, [w_A - h, w_B]) - z_s Q_s(T, [w_A]) \\ &+ \int d\mathbf{r} [h(\mathbf{r})\phi_{A,2}(\mathbf{r}) - \chi N\phi_A(\mathbf{r})\phi_B(\mathbf{r})]. \end{aligned} \quad (18)$$

Because the system is constrained to have a different concentration of hexagonal-formers in the cis leaf than in the trans leaf, its free energy will clearly be greater than if it were not so constrained. This is also true of the free energies of the various intermediates, like the stalk, hemifusion diaphragm, and pore. For the fusion process, however, we are interested in differences in free energies between the intermediates and the flat bilayers, and these differences can certainly be less in the constrained system.

4.1 Standard Mechanism

The calculations for the standard mechanism are relatively straightforward due to the axial and reflection symmetry of the stalk, the hemifusion diaphragm, and the pore. We need only indicate where the field $h(\mathbf{r})$ is non-zero, which is shown in Fig. 7. Specifically

$$\begin{aligned} h(\mathbf{r}) = h(z, \rho) &= h_0 & |z| \leq 0.6R_g \text{ and } \rho \geq R + 0.6R_g, \\ &= 0 & \text{otherwise,} \end{aligned} \quad (19)$$

with R the radius of the hemifusion diaphragm defined previously (17).

In Fig. 8 we show results for a bilayer under a tension $\gamma/\gamma_0 = 0.2$ composed of the lamellae-former which comprises a fraction $\phi_1 = 0.650$ of the bilayer by volume, and the hexagonal-former comprising a fraction $\phi_2 = 0.350$ by volume. Results are presented for the excess free energy of the hemifusion diaphragm (solid lines) and of the fusion pores (dashed lines) for different volume fractions in the cis leaf of the hexagonal-forming amphiphile. In the upper set of curves, there is no asymmetry, so that the volume fraction of hexagonal former in the cis leaf, $\phi_2^{cis} = 0.350$, is the same as in the whole bilayer. In the middle curve, the volume fraction of the hexagonal former in the cis leaf, has been increased to $\phi_2^{cis} = 0.395$. Its volume fraction in the trans leaf is concomitantly reduced to $\phi_2^{trans} = 0.305$, and the volume fractions of the lamellae-former in the cis and trans leaves are 0.605 and 0.695, respectively. In the lowest curve, we have set $\phi_2^{cis} = 0.431$, so that $\phi_2^{trans} = 0.269$,

and the volume fractions of the lamellae-former in the cis and trans leaves is 0.569 and 0.731. The barrier to fusion is reduced from $11k_B T$ to $8.5k_B T$, to $5k_B T$ as the asymmetry increases. For the largest asymmetry shown, the barrier to fusion is essentially no greater than the barrier to formation of the initial stalk itself.

4.2 Stalk/hole mechanism

We have calculated the barrier to fusion between asymmetric bilayers in the second stalk-hole mechanism. We have chosen this path, rather than the first stalk-hole mechanism, because the latter involves the calculation of the free energy of a hole in an asymmetric bilayer and of a hemifusion diaphragm which consists of the cis and trans layer of one of the original bilayers. As the bilayer is not symmetric, neither is the hemifusion diaphragm, and this lack of symmetry about the x, y plane makes the calculation rather slow. The second stalk-hole mechanism does not involve this asymmetric hemifusion diaphragm, although it still involves holes in asymmetric bilayers. The calculation of the energies in this pathway is more rapid. We have already shown that there is not a great deal of difference in the barrier energies in the two pathways in symmetric bilayers, Fig. 6(a), and assume the same is true with asymmetric bilayers. If anything, we will overestimate the fusion barrier of the stalk-hole mechanism because, as we add hexagonal-formers, the barrier in the second stalk-hole pathway which we calculate will probably become somewhat larger than that in the first pathway, just as it is in the symmetric bilayer case, Fig. 6(a).

Our results for the barrier to fusion of asymmetric bilayers within the second stalk-hole mechanism are shown in Fig. 9. We have calculated them for bilayers in which the average volume fraction of hexagonal-formers in the entire bilayer is kept fixed at $\phi_2 = 0.350$, while the fraction of hexagonal-formers in the cis layer, ϕ_2^{cis} , takes the values $\phi_2^{cis} = 0.350$ (i.e. no asymmetry), $\phi_2^{cis} = 0.395$, and $\phi_2^{cis} = 0.431$. The barrier to fusion for this second stalk-hole pathway is shown by the triangles. The values of α at the saddle point in the fusion pathway are, $\alpha = 0.073$ for $\phi_2^{cis} = 0.350$, $\alpha = 0.174$ when $\phi_2^{cis} = 0.395$, and $\alpha = 0.18$ when $\phi_2^{cis} = 0.431$. These barriers to fusion are compared to those calculated in the standard mechanism and shown in squares. These values were shown previously in Fig.8. Finally, we also compare them with the free energies of the stalk, shown in circles.

We note that the small values of α in the stalk-hole mechanism imply

that the stalk does not have to elongate very much in order to nucleate the formation of the two holes which, when surrounded by the stalk, will become the fusion pore. (We recall that in surrounding the holes, the energy of the system is reduced as the line tensions of the bare holes are replaced by the lower line tension of a hole next to a stalk (13).) Hole formation is enhanced, and the barrier to fusion reduced, because the majority amphiphile, $\phi_1 = 0.65$, is a lamellae-former with $f = 0.4$. Furthermore the actual volume fraction of the lamellae-former near the rim of a hole will be larger than this because the amphiphiles are free to move within a leaf to that region where they will reduce the energy most. The increase of α with the fraction of hexagonal-formers in the cis leaf is readily understood. As the fraction of hexagonal-former in the cis leaf increases, the energy of a pore decreases, as noted previously. It follows from Eq. 12 that α , the fraction of the stalk-hole intermediate that resembles a pore, will increase.

5 Discussion

We have employed a model of a mixture of two amphiphiles, one which is a lamellae-former, the other a hexagonal-former. The ratio of their hydrophilic part to the entire molecule was chosen so that the first resembles DOPC and the latter resembles DOPE. The two have the same hydrophobic volumes, but different hydrophilic ones. We have solved the model within self-consistent field theory.

We first considered bilayers whose leaves have identical compositions, and added hexagonal-formers to each leaf equally. We examined the effect of this addition on the barrier to fusion as calculated in the standard mechanism, and the first and second stalk-hole mechanisms. The barrier energy is reduced significantly in the standard mechanism from about $24 k_B T$ with no hexagonal-formers to about $11 k_B T$ with a volume fraction of 0.35 hexagonal-formers. This is seen in Figs. 5 and 9. As noted earlier, (17), we expect that the energies in biological, lipid, membranes are higher by a factor of about 2.5 than in the block copolymer membranes which we consider. Thus the above barrier values would correspond to one of $60 k_B T$ being reduced to $28 k_B T$. The reduction in the fusion barrier of the standard mechanism is due to a reduction in the energy of the hemifusion intermediate, partly because the average number of hexagonal-formers has increased (16), and partly because the hexagonal-forming amphiphiles preferentially go to the

edge of the hemifusion diaphragm, as seen in Fig. 4. Fig. 5 shows that the greatest rate of decrease comes about when the hexagonal-formers are first added to the pure bilayer of lamellae-formers. This rapid decrease occurs because the hexagonal-formers go to the regions where they can most readily reduce the free energy. The distribution of the different amphiphiles are not spatially uniform when there are fusion intermediates. The reduction of the barrier energy in the stalk-hole mechanism, is more modest but not insignificant. In the second stalk-hole mechanism, it is reduced from $8.3 k_B T$ when there are no hexagonal-formers to $6.8 k_B T$ with a volume fraction of 0.350 hexagonal-formers. Again this would correspond to a reduction from $21 k_B T$ to $17 k_B T$.

We then examined the effect on the barrier to fusion of an unequal distribution of hexagonal- and lamellae-formers in the two leaves. We considered a system in which the hexagonal-formers make up a volume fraction of 0.350 of the whole system, much as they do in human red blood cell membranes. This brings about a further significant reduction in the barrier to fusion in both mechanisms. In the standard mechanism, this is due to the reduction in energy of the hemifusion diaphragm, while in the stalk-hole mechanism it is due primarily to the reduction in energy of the elongated stalk.

The energy of the initial stalk itself is not affected very much either by the addition of hexagonal-formers to each leaf equally, as seen in Fig. 3, nor by the redistribution of the hexagonal-formers between the two leaves, Fig. 9. The former result is in contrast to the prediction of phenomenological theories of a sensitive dependence upon the amount of hexagonal-formers, (16).

Certainly the most important result of our calculation is the following: although the fusion process remains one with two barriers, one due to stalk formation and another which depends upon the specific mechanism, the second barrier is rapidly reduced by the addition of hexagonal-former of greater abundance in the cis layer to a value comparable to that of the initial stalk itself. As emphasized earlier, the calculated energy of the stalk is rather small, on the order of $5 k_B T$ in our copolymer system, corresponding to $13 k_B T$ in a biological membrane.

We note that the volume fraction of hexagonal-former in the cis leaf at which the two barriers become approximately equal occurs in our model at a value of about $\phi_2^{cis} \sim 0.43$. The average fraction of hexagonal-formers in the bilayer is 0.35. Assuming equal molecular weights for the A and B components of the diblock, these volume fractions correspond to a mole fraction

of 0.47 in the cis leaf of a bilayer in which its average mole fraction is 0.39. Again, the mole fractions of hexagonal-formers in the membrane of human red blood cells is approximately 0.54 in the cis leaf and 0.35 when averaged over both leaves of the bilayer. Thus equality of the two barriers occurs in our model at a somewhat smaller asymmetry between leaves than occurs in red blood cell membranes. As the asymmetry increases, the second barrier to fusion continues to decrease and eventually becomes negative. When this occurs in a bilayer under zero surface tension, the bilayer is unstable. In the system shown in Fig. 9, this instability occurs at a mole fraction of hexagonal-former in the cis layer of about 0.50.

To reiterate, our major result is that the two barriers to fusion are *comparable* and *small* for an amount of hexagonal-former found in the cis layer which does not differ greatly from that found in red blood cell membranes. If this result is applicable to biological membranes, then there are important implications. The first is that fusion should proceed readily once external sources have brought the membranes sufficiently close to initiate the process. This shifts the focus of fusion to an understanding of those mechanisms which bring this about. The second is an emphasis on the caution which must be exercised when extrapolating to the fusion of biological membranes the experimental or theoretical results gleaned from fusion studies of non-biological membranes with leaves of equal compositions.

We are grateful to Kirill Katsov for useful correspondence. This work was supported by the National Science Foundation under grant No. 0503752.

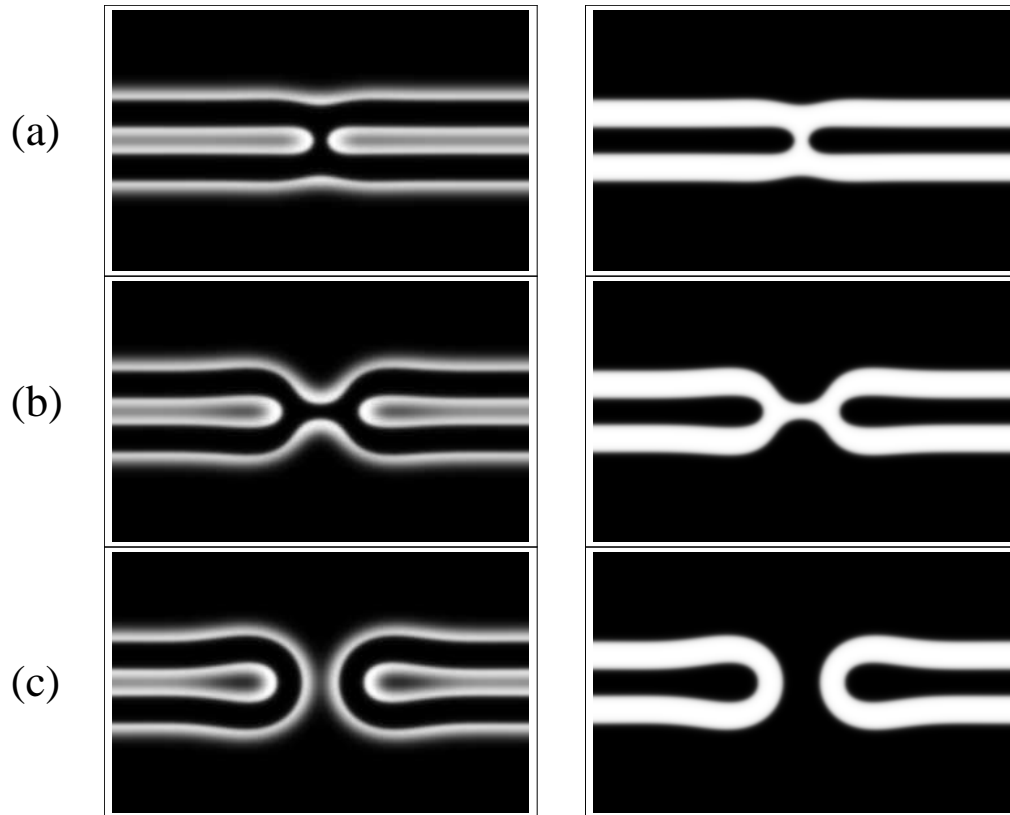


Figure 1:

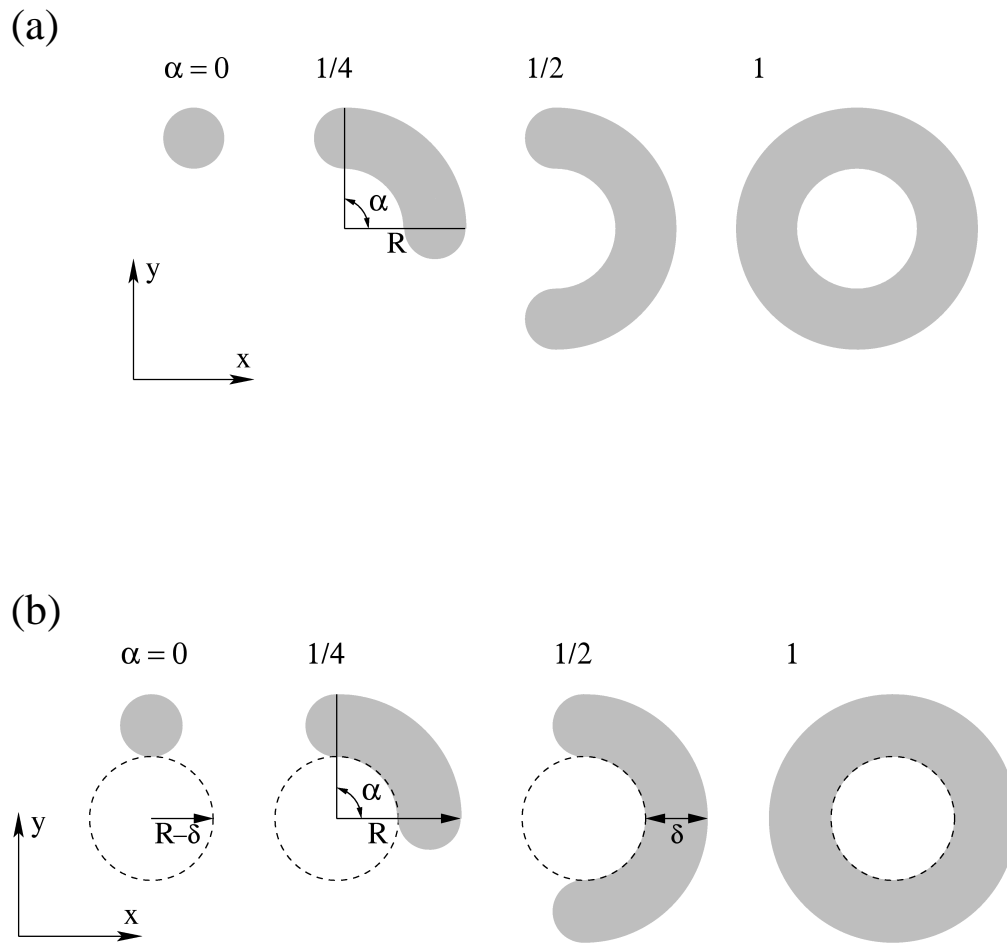


Figure 2:

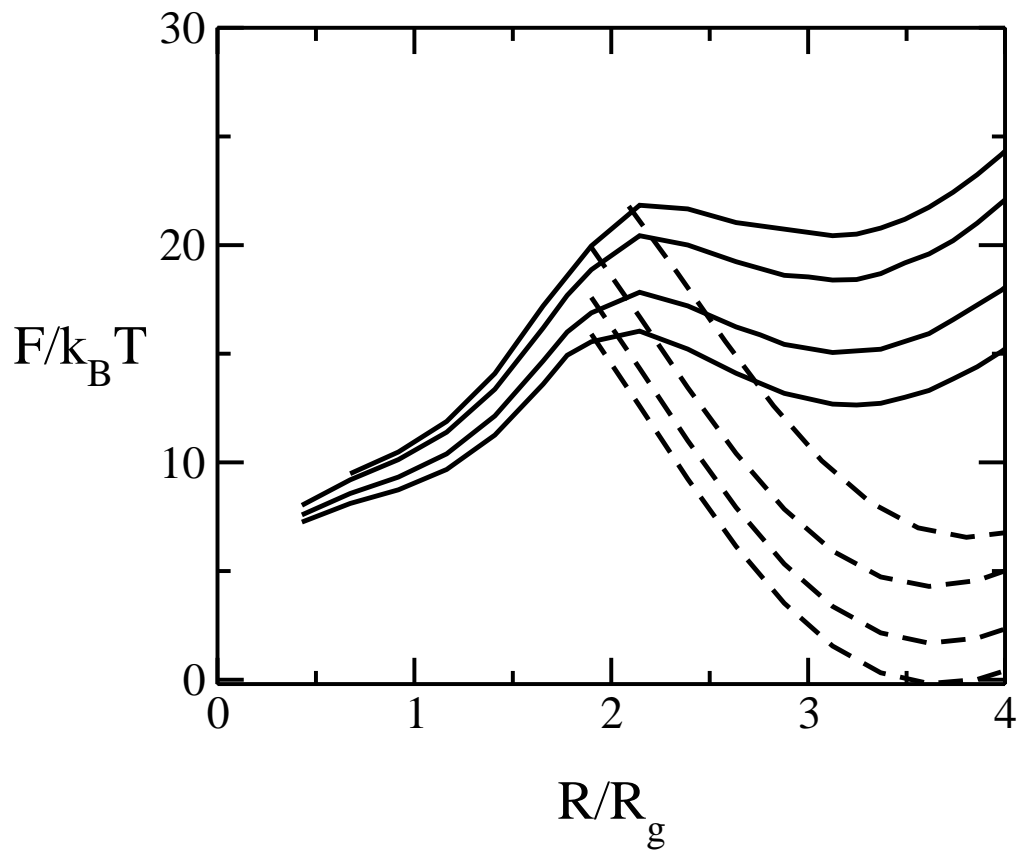


Figure 3:

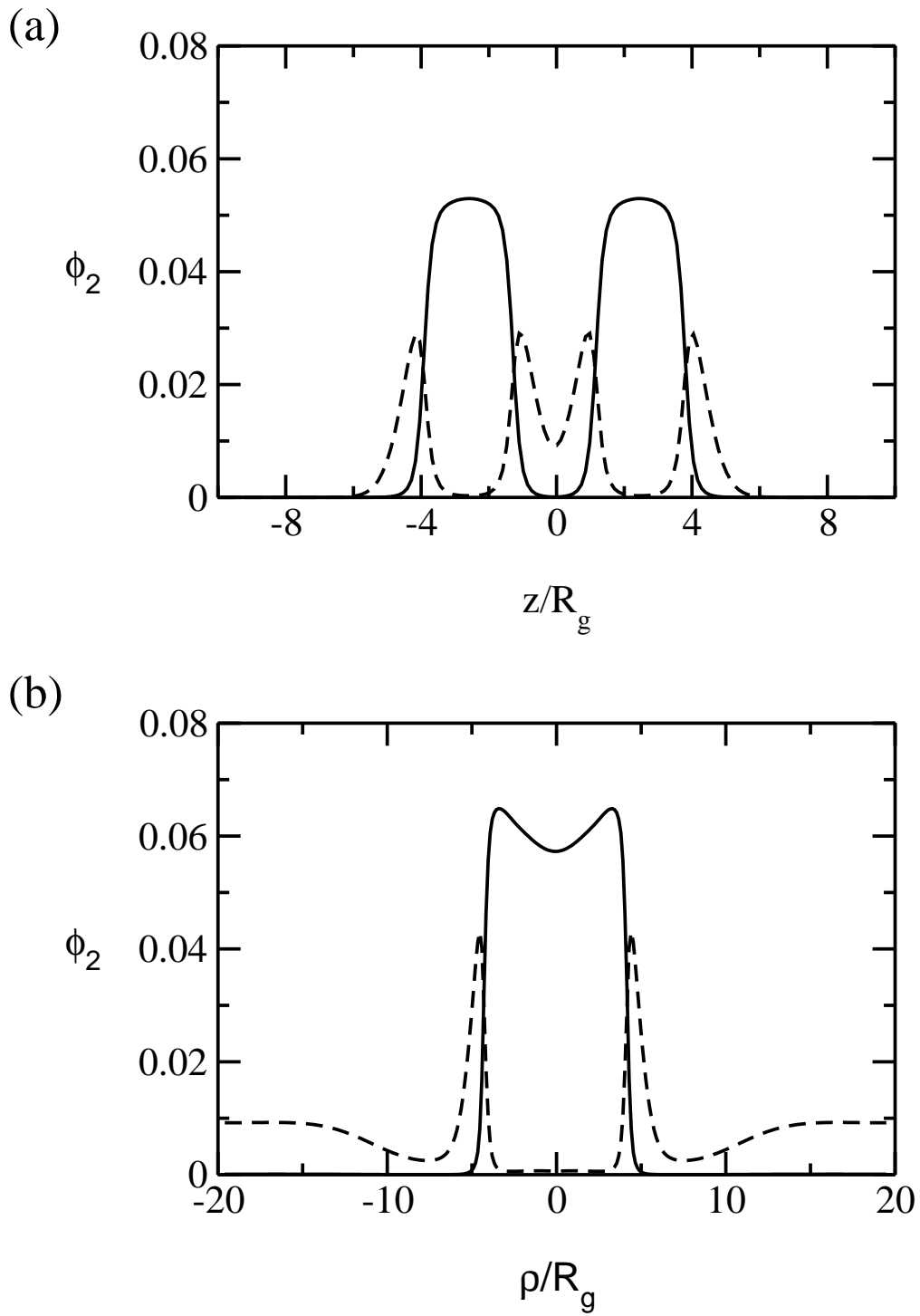


Figure 4:
20

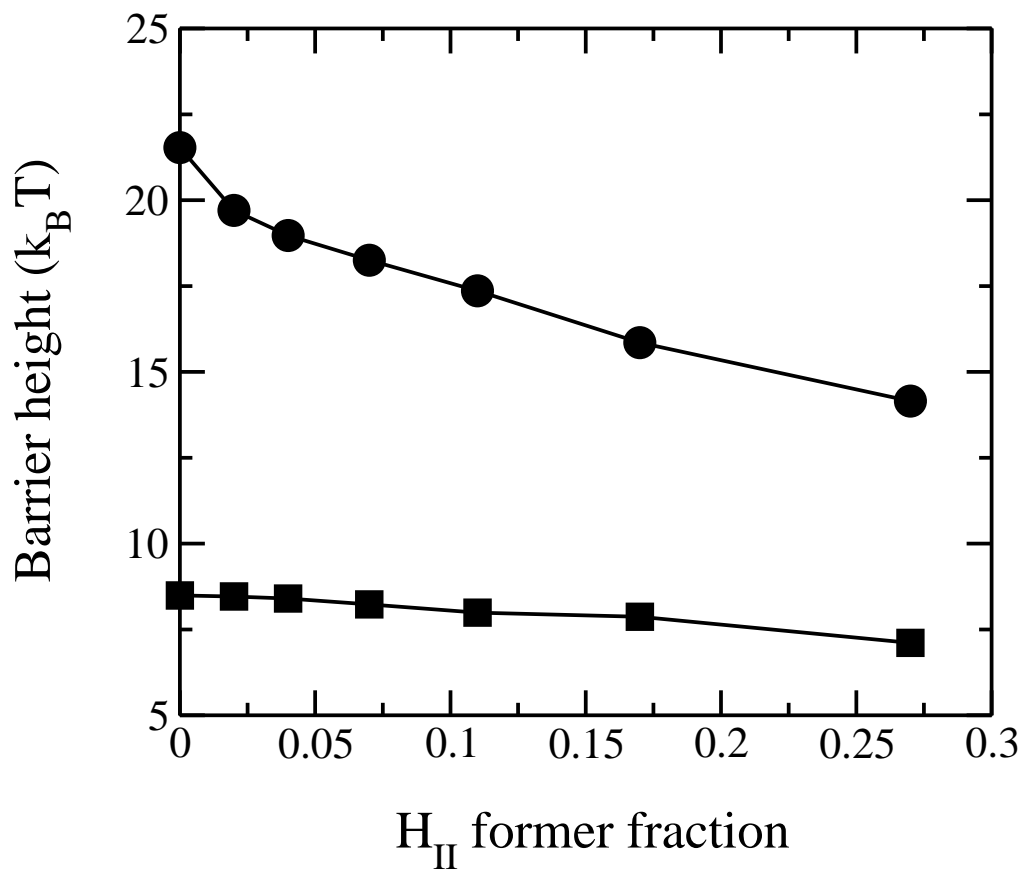
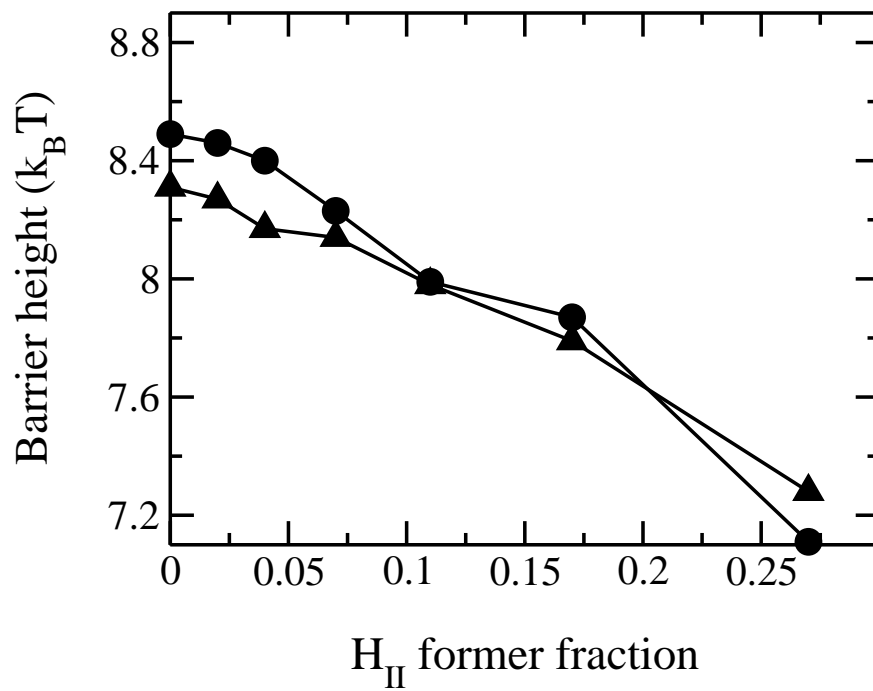


Figure 5:

(a)



(b)

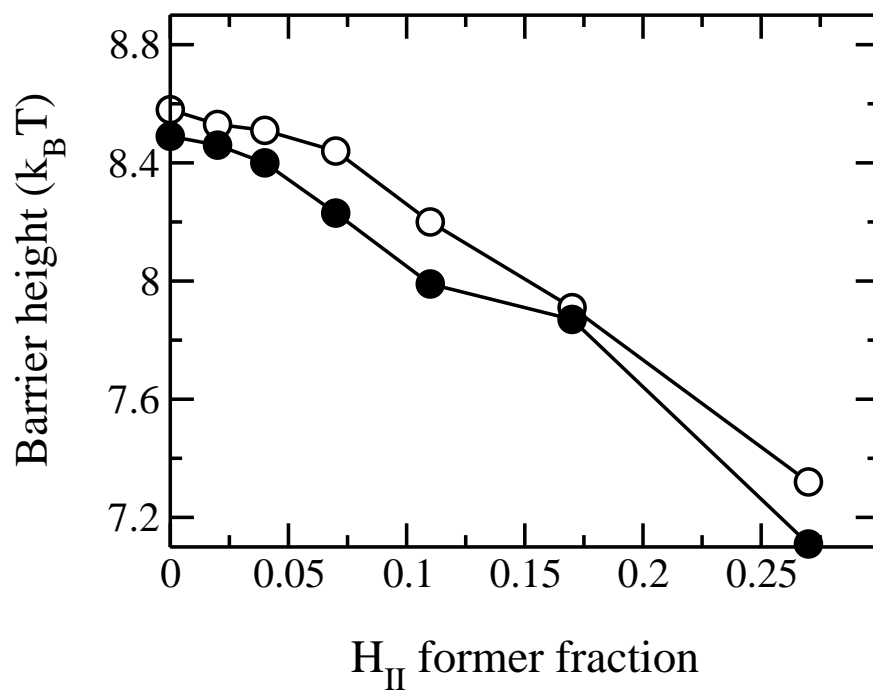


Figure 6:

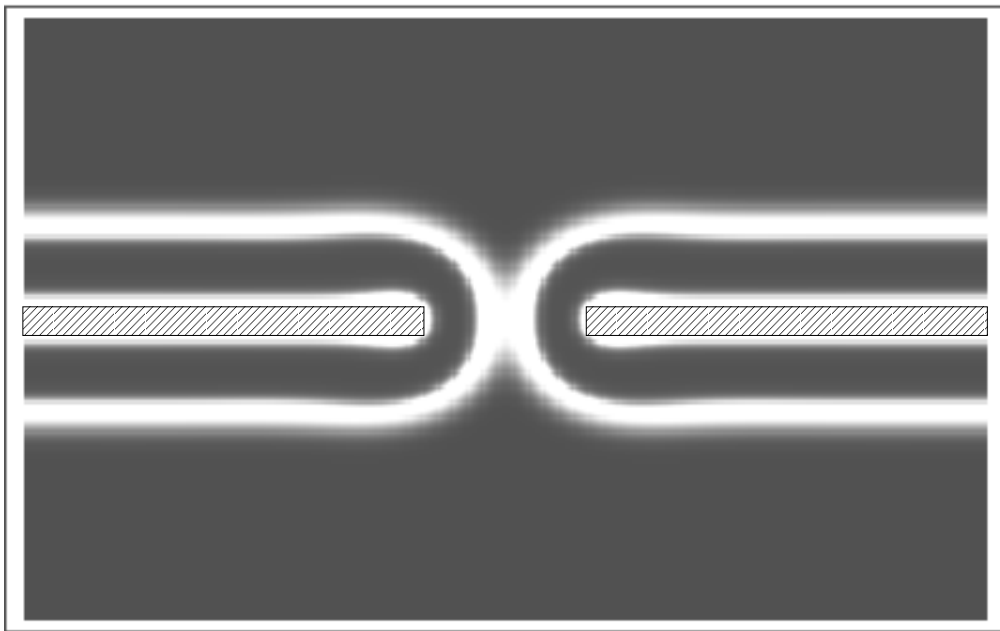


Figure 7:

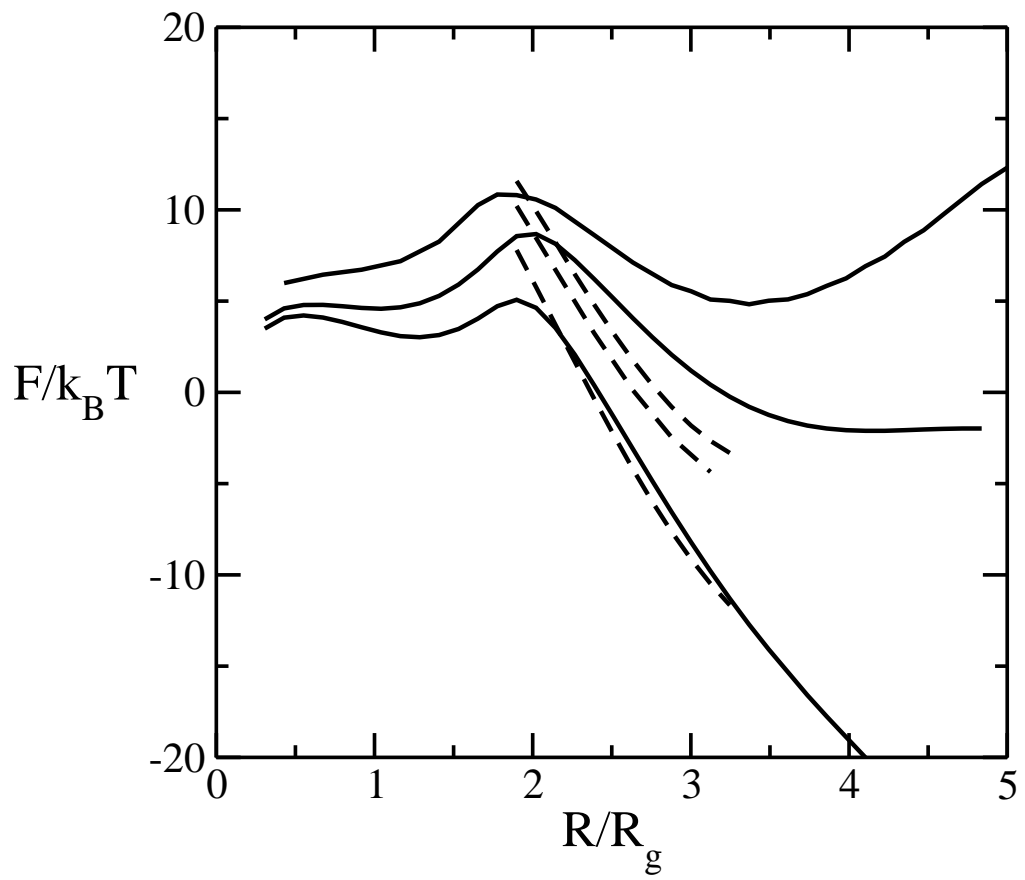


Figure 8:

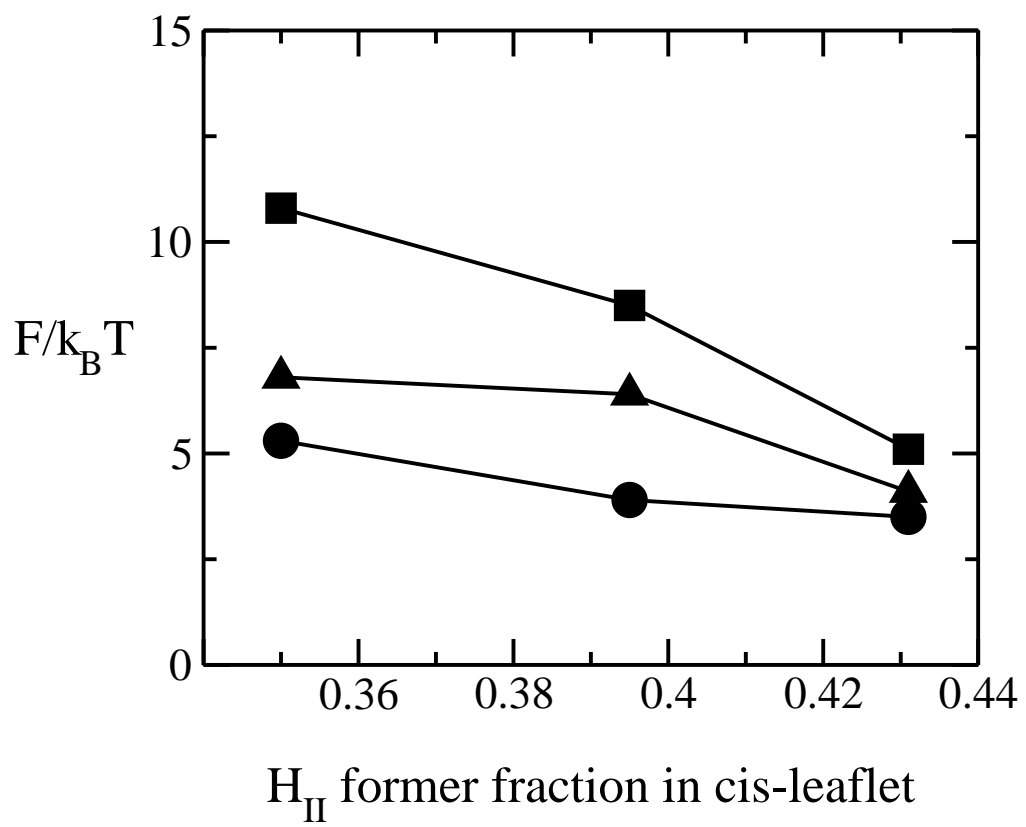


Figure 9:

6 Figure Captions

Figure 1. The standard stalk model description of membrane fusion. Light regions indicate the areas of head groups of the bilayer in the left-hand panel, and of tail groups in the right-hand panel. (a) stalk (b) hemifusion diaphragm (c) fusion pore.

Figure 2. (a) Parameterization of the elongated stalk. The shading schematically shows the location of the hydrophobic segments in the plane of symmetry between fusing bilayers. The arc radius R corresponds to the radial distance to the outer hydrophilic/hydrophobic interface in the plane of symmetry. Values of the fractional arc angle, α , defined in the range $[0,1]$, are given at the top of each stalk configuration. Note that $\alpha = 0$ corresponds to the original stalk configuration. (b) Parameterization of the stalk-hole complex. In the first stalk-hole mechanism, there is a hole in one bilayer and the projection of its edge is shown with a dashed line. In the second stalk-hole mechanism, there is a hole in each of the bilayers, and the dashed line represents the projection of their edges. The radius of the hole, or holes, is $R - \delta$. The hydrophobic thickness of the bilayer is δ . Values of the fractional arc angle, α , defined in the range $[0,1]$, are given at the top of each configuration.

Figure 3. Excess free energies of fusion intermediates in the standard model are shown at a tension of $\gamma/\gamma_0 = 0.2$. Solid curves indicate stalk/hemifusion intermediates and dashed curves fusion pores. The bilayers consist of AB diblocks of two different lengths and architectures. The first diblock is described by N segments and $f_1 = 0.4$, and the second diblock by $\tilde{\alpha}N$ segments with $\tilde{\alpha}_2 = 0.85$ and $\tilde{\alpha}_2(1 - f_2) = 0.6$. From top to bottom, the volume fractions of type 2 diblocks in the bilayers are 0.00, 0.04, 0.11, and 0.17.

Figure 4. (a) Volume fractions, ϕ_2 , of the head group, dashed line, and tail, solid line, of the hexagonal-forming amphiphile in the bilayers far from the hemifusion diaphragm are shown in a cut perpendicular to the bilayers as a function of the dimensionless vertical coordinate z/R_g . (b) These same volume fractions are shown in the $z = 0$ plane of symmetry which passes through the hemifusion diaphragm itself as a function of

the dimensionless radial coordinate ρ/R_g . The hemifusion diaphragm has a radius of about $5R_g$.

Figure 5. Barrier height of fusion process as a function of the volume fraction of the hexagonal-forming (H_{II}) amphiphile. The upper curve shows the barrier heights in the standard stalk-hemifusion mechanism. The lower curve shows the barrier heights in the first stalk-hole mechanism with a defect energy of $F_d = 4k_B T$.

Figure 6.(a) Comparison of the barrier to fusion in the first (filled circles) and second (filled triangles) stalk-hole mechanisms as a function of volume fraction of hexagonal-forming (H_{II}) amphiphile. (b) Comparison of barrier to fusion in the first stalk-hole mechanism with defect energy of $4k_B T$ (open circles) and vanishing defect energy (closed circles).

Figure 7. Density profile of a fusion pore. The region where external fields are applied to maintain asymmetry is marked by shaded areas on the density plot of small head groups. White regions indicate the areas where small head groups are concentrated and the gray regions the areas in which their concentration is strongly reduced.

Figure 8. Excess free energies of standard fusion intermediates for bilayers of the same overall composition, but with varying transbilayer distributions under $\gamma/\gamma_0 = 0.2$ tension. The bilayers here contain 65% lamellae-forming diblock and 35% hexagonal-forming diblock. The solid curves represent excess free energies of stalk/hemifusion diaphragm and the dashed curves excess free energies of fusion pores. In the upper set of curves, there is no asymmetry, so that the volume fraction of hexagonal former in the cis leaf, $\phi_2^{cis} = 0.350$, is the same as in the whole bilayer. In the middle curve, the volume fraction of the hexagonal former in the cis leaf, has been increased to $\phi_2^{cis} = 0.395$. In the lowest curve, we have set $\phi_2^{cis} = 0.431$. The barrier to fusion is reduced from $11k_B T$ to $8.5k_B T$, to $5k_B T$ as the asymmetry increases.

Figure 9. Comparison of the barrier to fusion of asymmetric bilayers containing an average volume fraction of hexagonal-formers of $\phi_2 = 0.35$ as calculated along the standard pathway, (squares), and the second stalk-hole pathway, (triangles) for three different volume fractions

of hexagonal-formers in the cis layer; $\phi_2^{cis} = 0.350, 0.395, 0.431$. Also shown is the free energy of a stalk, (circles), in the same systems.

References

1. Chernomordik, L. V., and M. M. Kozlov. 2003. Protein-lipid interplay in fusion and fission of biological membranes. *Annu. Rev. Biochem* 72:175–207.
2. Cohen, F. S., and G. B. Melikyan. 2004. The energetics of membrane fusion from binding, through hemifusion, pore formation, and pore enlargement. *J. Membrane Biol.* 199:1–14.
3. Evans, K. O., and B. R. Lentz. 2002. Kinetics of lipid rearrangements during poly(ethylene glycol)-mediated fusion of highly curved unilamellar vesicles. *Biochemistry* 41:1241–1249.
4. Kozlov, M. M., and V. S. Markin. 1983. Possible mechanism of membrane fusion. *Biofizika* 28:255–261.
5. Müller, M., K. Katsov, and M. Schick. 2002. New mechanism of membrane fusion. *J. Chem. Phys.* 116:2342–2345.
6. Müller, M., K. Katsov, and M. Schick. 2003. A new mechanism of model membrane fusion determined from monte carlo simulation. *Biophys. J.* 85:1611–1623.
7. Stevens, M. J., J. Hoh, and T. Woolf. 2003. Insights into the molecular mechanism of membrane fusion from simulation: evidence for the association of splayed tails. *Phys. Rev. Lett.* 91:188102–1–188102–4.
8. Marrink, S. J., and A. E. Mark. 2003. The mechanism of vesicle fusion as revealed by molecular dynamics simulations. *J. Am. Chem. Soc.* 125:11144–11145.
9. Smeijers, A. F., A. J. Marvoort, K. Pieterse, and P. A. J. Hilbers. 2006. A detailed look at vesicle fusion. *J. Phys. Chem. B* 110:13212–13219.
10. Siegel, D. P. 1993. Energetics of intermediates in membrane fusion: comparison of stalk and inverted micellar intermediate mechanisms. *Biophys. J.* 65:2124–2140.
11. Kuzmin, P. I., J. Zimmerberg, Y. A. Chizmadzhev, and F. S. Cohen. 2001. A quantitative model for membrane fusion based on low-energy intermediates. *Proc. Natl. Acad. Sci. U.S.A.* 98:7235–7240.

12. Noguchi, H., and M. Takasu. 2001. Fusion pathways of vesicles: A brownian dynamics simulation. *J. Chem. Phys.* 115:9547–9551.
13. Katsov, K., M. Müller, and M. Schick. 2006. Field theoretic study of bilayer membrane fusion: II. mechanism of a stalk-hole complex. *Biophys. J.* 90:915–926.
14. Lentz, B. 2006. Seeing is believing: The stalk intermediate. *Biophys. J.* 91:BioFAST.
15. Markin, V. S., and J. P. Albanesi. 2002. Membrane fusion: stalk model revisited. *Biophys. J.* 82:693–712.
16. Kozlovsky, Y., and M. M. Kozlov. 2002. Stalk model of membrane fusion: solution of energy crisis. *Biophys. J.* 82:882–895.
17. Katsov, K., M. Müller, and M. Schick. 2004. Field theoretic study of bilayer membrane fusion: I. hemifusion mechanism. *Biophys. J.* 87:3277–3290.
18. Rothman, J. E., and J. Lenard. 1977. Membrane asymmetry. *Science* 195:743–753.
19. Devaux, P. 1991. Static and dynamic lipid asymmetry in cell membranes. *Biochemistry* 30:1163–1173.
20. Seigneuret, M., and P. F. Devaux. 1984. Asymmetric distribution of spin-labeled phospholipids in the erythrocyte membrane: Relation to shape changes. *Proc. Natl Acad. Sci. USA* 81:3751–3755.
21. Eastman, S., M. J. Hope, K. Wong, and P. R. Cullis. 1992. Influence of phospholipid asymmetry on fusion between large unilamellar vesicles. *Biochemistry* 31:4262–4268.
22. Bailey, A. L., and P. R. Cullis. 1994. Modulation of membrane fusion by asymmetric transbilayer distributions of amino lipids. *Biochemistry* 33:12573–12580.
23. Chernomordik, L., M. Kozlov, and J. Zimmerberg. 1995. Lipids in biological membrane fusion. *J. Membr. Biol.* 146:1–14.

24. Hope, M. J., and P. R. Cullis. 1980. Effects of divalent cations and *ph* on phosphatidylserine model membranes: A ^{31}P nmr study. *Biochem. and Biophys. Res. Comm.* 92:846–852.
25. Gruner, S. M. 1989. Stability of lyotropic phases with curved interfaces. *J. Phys. Chem.* 93:7562–1570.
26. Siegel, D. P. 1986. Inverted micellar intermediates and the transitions between lamellar, inverted hexagonal, and cubic lipid phases. ii. implications for membrane-membrane interactions and membrane fusion. *Biophys. J.* 49:1171–1183.
27. Hope, M. J., W. D. C, and P. Cullis. 1983. Ca^{2+} and *ph* induced fusion of small unilamellar vesicles consisting of phosphatidylethanolamine and negatively charged phospholipids: a freeze fracture study. *Biochem. Biophys. Res. Commun.* 110:15–22.
28. Kozlovsky, Y., L. V. Chernomordik, and M. M. Kozlov. 2002. Lipid intermediates in membrane fusion: formation, structure, and decay of hemifusion diaphragm. *Biophys. J.* 83:2634–2651.
29. Li, X.-J., and M. Schick. 2000. Distribution of lipids in nonlamellar phases of their mixtures. *J. Chem. Phys.* 112:6063–6072.
30. Loison, C., M. Mareschal, and F. Schmid. 2004. Pores in bilayer membranes of amphiphilic molecules: Coarse-grained molecular dynamics simulations compared with simple mesoscopic models. *J. Chem. Phys.* 121:1890–1900.
31. Tolpekina, T., W. den Otter, and W. Briels. 2004. Simulations of stable pores in membranes: System size dependence and line tension. *J. Chem. Phys.* 121:8014–8020.
32. Tieleman, D., H. Leontiadou, A. Mark, and S. Marrink. 2003. Simulation of pore formation in lipid bilayers by mechanical stress and electric fields. *J. Am. Chem. Soc.* 125:6382–6383.
33. Leontiadou, H., A. Mark, and S. Marrink. 2004. Molecular dynamics simulations of hydrophilic pores in lipid bilayers. *Biophys. J.* 86:2156–2164.

34. Groot, R., and K. Rabone. 2001. Mesoscopic simulation of cell membrane damage, morphology change and rupture by nonionic surfactants. *Biophys. J.* 81:725–736.